Environmental Science and Pollution Research (2023) 30:85626–85638
https://doi.org/10.1007/s11356-023-28385-0

RESEARCH ARTICLE

Photocatalytic performance of PANI modified TiO_2: Degradation of refractory organic matter

Ceyda S. Uyguner-Demirel[1] · Nazli Turkten[2] · Yunus Karatas[2] · Miray Bekbolet[1]

Received: 16 April 2023 / Accepted: 18 June 2023 / Published online: 30 June 2023

Abstract

Surface modification of TiO_2 with polyaniline (PANI) conducting polymer has been used to achieve visible light photoresponse, thereby increasing solar photocatalytic activity. In this study, photocatalytic performances of PANI-TiO_2 composites with different mole ratios were synthesized by the in situ chemical oxidation polymerization method and tested for the degradation of a model refractory organic matter (RfOM), namely humic acid in an aqueous medium under simulated solar irradiation in a comparative manner. Adsorptive interactions under dark conditions and interactions under irradiation were investigated as contributing factors to photocatalysis. Degradation of RfOM was monitored in terms of UV–vis parameters ($Color_{436}$, UV_{365}, UV_{280}, and UV_{254}) and fluorescence spectroscopic parameters as well as the mineralization extent by dissolved organic carbon contents. The presence of PANI exerted an enhancement in photocatalytic degradation efficiency compared to pristine TiO_2. The synergistic effect was more pronounced in lower PANI ratios whereas higher PANI ratios reflected a retardation effect. Degradation kinetics were assessed by pseudo-first-order kinetic model. For all UV–vis parameters analyzed, highest and lowest rate constants (k) were attained in the presence of PT-14 (2.093×10^{-2} to 2.750×10^{-2} min^{-1}) and PT-81 (5.47×10^{-3} to 8.52×10^{-3} min^{-1}), respectively. Variations in selected absorbance quotients, i.e., A_{254}/A_{436}, A_{280}/A_{436}, and A_{253}/A_{203}, were distinctive and compared with respect to irradiation time and photocatalyst type. Upon use of PT-14, a steady decreasing profile with respect to irradiation time was attained for A_{253}/A_{203} quotient as 0.76–0.61, followed by a rapid decrease to 0.19 in 120 min. The incorporation effect of PANI into TiO_2 composite could be visualized in A_{280}/A_{365} and A_{254}/A_{365} quotients exhibiting an almost constant and parallel trend. As a general trend, decrease in the major fluorophoric intensity $FI_{syn,470}$ with photocatalysis was observed under extended irradiation conditions; however, an abrupt decline was remarkable in the presence of PT-14 and PT-18. Fluorescence intensity decrease correlated well with spectroscopic evaluation of rate constants. A thorough evaluation of spectroscopic parameters of UV–vis and fluorescence can provide significant information for practical applications in control of RfOM in water treatment.

Keywords Degradation kinetics · Photocatalysis · PANI-TiO_2 composite · Refractory organic matter

Introduction

Due to the continuous release of contaminants into the environment, the application of photocatalysis as an alternative advanced oxidation treatment process is attracting the focus of researchers. As presented for decades, TiO_2 is the most extensively used photocatalyst exhibiting excellent photocatalytic activity, stability, and a band gap energy ($E_{bg}=3.2$ eV) coinciding with UVA region of solar spectrum (Parrino and Palmisano 2021).

To overcome the disadvantages of n-type semiconductors expressing large band gaps, coupling with conducting polymers (CPs) that exhibit small bandgaps and extended π–e^- systems drew current interest. With respect to attained beneficial effect via "sensitization," coupling of p-type conducting polymers with an n-type semiconductor is regarded as a new area of research. Polyaniline (PANI), primarily composed of benzenoid and quinoid structures, is the most widely studied CP. The combination of PANI (p-type CP) with

Responsible Editor: George Z. Kyzas

✉ Ceyda S. Uyguner-Demirel
uygunerc@boun.edu.tr

[1] Institute of Environmental Sciences, Bogazici University, Bebek, Istanbul 34342, Turkey

[2] Department of Chemistry, Faculty of Arts and Sciences, Kirsehir Ahi Evran University, Kirsehir 40100, Turkey

TiO_2 (n-type semiconductor) as a p–n junction reduces the rate of electron–hole recombination leading to enhancement in photocatalytic activity. Hence, for photocatalytic applications, PANI has been reported as a suitable candidate for the preparation of PANI-TiO_2 composites (Nowakowska and Szczubiałka 2017; Riaz et al. 2015).

The photocatalytic activity of PANI/TiO_2 composite has been investigated using various substrates covering dyes, i.e., methylene blue (Deng et al. 2016; Doğan et al. 2020; Heshmatpour and Zarrin 2017; Koysuren and Koysuren 2019; Lee et al. 2020; Rahman and Kar 2020a, b; Reddy et al. 2016; Yang et al. 2017), reactive red 45 (Gilja et al. 2017), reactive black 5 (Jumat et al. 2017), rhodamine B (Deng et al. 2016; Ma et al. 2020; Reddy et al. 2016), methyl orange (Sboui et al. 2017), crystal violet (Heshmatpour and Zarrin 2017), allura red, and quinoline yellow (Salem et al. 2009); various pesticides such as thiacloprid, clomazone, quinmerac, and sulcotrione (Lazarevic et al. 2019); emerging contaminants, e.g., bisphenol A (Rahman and Kar 2020a; Sambaza et al. 2020) and sulfaquinoxaline (Sandikly et al. 2021); and as an example of microbiological species bacteriophage MS2 was also studied. A comprehensive study on the removal of selected biologically active compounds (pharmaceuticals and pesticides) was also performed by Merkulov and colleagues reporting degradation kinetics, toxicity evaluation, as well as assessment of reaction intermediates (Sojic Merkulov et al. 2018). Detailed information about various light sources utilized in related studies in literature was reported by Turkten and colleagues (Turkten et al. 2021).

The presence and role of organic matter (NOM) in natural terrestrial and aquatic environments has long been investigated due of its ill-defined composition, molecular size polydispersity, and configurational diversity (Feng et al. 2022). Possessing relatively poor biodegradability, organic matter could also be defined as refractory organic matter (RfOM) (Frimmel et al. 2008). RfOM is mainly composed of organic fractions as humic substances, which can further be classified as humic acid (HA), fulvic acids, and humin. Humic macromolecules are composed of conjugated olefinic, aromatic, phenolic–semiquinone–quinone structures expressing a wide spectrum of aliphatic/aromatic functional groups and chromophoric moieties.

The presence of these substances is mainly considered from aesthetic problems, i.e., color, although the major health concern is related to the formation of potentially harmful disinfection by-products. Therefore, removal of organic matter from drinking water holds prime importance achieved either by conventional methods or by advanced oxidation processes. Extensive efforts were devoted to unravel the interactions between NOM/RfOM and TiO_2 in relation to direct photocatalytic abatement of organic matrix in natural waters (Drosos et al. 2015; Tercero Espinoza et al. 2009; Uyguner-Demirel and Bekbolet 2011; Uyguner-Demirel et al. 2017). Recent interest was mainly diverted to testing bare and Cu-doped TiO_2 specimens for the photocatalytic removal of various molecular size fractions of HA as the representative of organic matter (Turkten et al. 2019; Uyguner-Demirel et al. 2022). Moreover, 100 kDa HA and its reactivity towards visible light active TiO_2/ZnO composite photocatalyst specimens was also investigated (Turkten and Bekbolet 2020).

Preparation of PANI composites and their applications for photocatalysis by our research group are mostly on the removal of simple organic dyes such as like methylene blue as standards for material testing in aqueous medium under UVA irradiation (Turkten et al. 2021). As a further step, this study was conducted to gain insight about the activities of PANI-TiO_2 composites for the removal of complex refractory organic matter (RfOM) namely HA. In recent years, a few studies were reported on the photocatalytic removal performance of both anionic and cationic dyes such as malachite green (Sarmah and Kumar 2011), methylene blue (Koysuren and Koysuren 2019; Turkten et al. 2021), malachite green and methylene blue (Eskizeybek et al. 2012), and organic pollutants such as phenol (Cui et al. 2018) in aqueous medium using PANI specimen. Moreover, there were several adsorption studies using PANI/HA composites for the removal of heavy metals in water (Li et al. 2011; Zhang et al. 2010). Besides, Wang and his colleagues investigated PANI as adsorbent to remove HA in aqueous solution (Wang et al. 2012). The photocatalytic degradation mechanism of many simple model compounds the structures of which are well known, are used for photocatalytic activity testing in the presence of PANI. The degradation kinetics and mechanisms of these basic compounds can be predicted according to related literature findings. However, in case of complex RfOM whose molecular structure is unknown, there are many other effects that are directly associated with the properties of humic acid like its origin (aquatic, terrestrial, etc.), polydisperse structure effecting its molecular size fraction and photosensitization property. Moreover, operational parameters like photocatalyst type, effective light wavelength, pH, and medium composition should also be considered in photocatalysis. Hence, investigating the photocatalytic degradation of RfOM in the presence of PANI-TiO_2 composites requires significant interest. To the best of our knowledge, photocatalytic performances of PANI and PANI-TiO_2 composites for the degradation of RfOM in aqueous medium were reported for the first time in this study under simulated solar irradiation in a comparative manner. Detailed information on the preparation and characterization of PANI and PANI-TiO_2 composites was presented elsewhere (Turkten et al. submitted for publication). The adsorptive interactions under dark conditions and interactions under irradiation as contributing factors to photocatalysis were also highlighted. RfOM removal was

followed by selected UV–vis parameters ($Color_{436,}$ UV_{365}, UV_{280}, and UV_{254}), specific UV–vis quotients (A_{254}/A_{436}, $A_{280}/A_{436,}$ A_{254}/A_{365}, A_{280}/A_{365}, and A_{253}/A_{203}) and fluorescence spectroscopy (synchronous scan) under dark and irradiation conditions. In this regard, the multicomponent interaction mechanism prevailing between PANI, RfOM, and TiO_2 or the resulting possible structural changes of the ternary system were not the focus of this study.

Methodology

Materials and Methods

TiO_2 P-25 supplied from Evonik was used as the primary photocatalyst (referred to simply as TiO_2). Aniline ($C_6H_5NH_2$, for analysis), ammonium persulfate ($(NH_4)_2S_2O_8$ ACS reagent, ≥ 98.0%), and hydrochloric acid (HCl, ACS reagent, 37%) were provided by Merck and used without further purification. Humic acid (HA) was purchased from Aldrich (Sigma-Aldrich, St. Louis, MO, USA) as sodium salt. All aqueous solutions were prepared with deionized water.

The emeraldine salt (conducting) form of PANI (referred to simply as PANI) and PANI-TiO_2 composites were synthesized by in situ chemical oxidation polymerization method. The synthesis procedure was explained in Part I of the study (Turkten et al. submitted for publication). A representative chemical structure of PANI was illustrated in Supplementary Materials (SM) in Fig. SM1. PANI-TiO_2 composites were designated as PT-18, PT-14, PT-11, PT-41, and PT-81, respectively, based on their relative mole ratios. All PT specimens were characterized according to Fourier transform infrared spectroscopy, Raman spectroscopy, X-ray diffraction, scanning electron microscopy, X-ray photoelectron spectroscopy, diffuse reflectance spectroscopy, photoluminescence spectroscopy, Brunauer–Emmett–Teller surface area, and thermo-gravimetric analyses techniques as presented by Turkten and colleagues (Turkten et al. submitted for publication). The surface characteristic properties of PANI, TiO_2, and PT-11 are presented in SM, Table SM1.

Preparation methodology of RfOM model compound

RfOM representative model compound was prepared as 100 kDa molecular size fraction of HA by stirred cell ultrafiltration apparatus (Amicon 8050) using appropriate membrane filter cutoff. Distilled-deionized water was used where necessary. The specified UV–vis parameters and dissolved organic carbon (DOC) content of 100 kDa HA were determined as follows: $Color_{436} = 0.107$, $UV_{365} = 0.227$, $UV_{280} = 0.547$, $UV_{254} = 0.640$, and DOC = 7.294 mg L^{-1} (Birben et al. 2017).

Assessment of photocatalytic activity

Photocatalytic activity testing was performed using Solar Simulator Atlas Suntest CPS + (Ref. 56,052,371) equipped with an air-cooled Xenon lamp with emission range of $\lambda = 300–800$ nm and light intensity of $I_o = 250$ W m^{-2}. The photocatalyst dose was kept constant as 0.25 mg mL^{-1}. All runs were performed individually using 50 mL sample volume. The experiments were performed at room temperature (25 °C ± 2) and under non-adjusted pH conditions (pH = 5.5–6.0). The stirring speed of the magnetic stirrer was also set to 320 rpm avoiding vortex formation. Irradiation time-based changes of RfOM were monitored according to descriptive parameters outlined in the following section.

Selected RfOM descriptive parameters

UV–vis spectroscopic parameters A Perkin Elmer Lambda 35 spectrophotometer was used for the measurement of absorbance at specific wavelengths of 436 nm ($Color_{436}$), 365 nm (UV_{365}), 280 nm (UV_{280}), and 254 nm (UV_{254}). UV–vis absorbance quotients as A_{254}/A_{436}, $A_{280}/A_{436,}$ A_{254}/A_{365}, A_{280}/A_{365}, and A_{253}/A_{203} were also presented. The photocatalytic activities were evaluated with respect to the degradation kinetics of RfOM as expressed by selected UV–vis parameters ($Color_{436}$, UV_{365}, UV_{280}, and UV_{254}). The differentiations were acquired in terms of the absorbance values in color forming moieties ($Color_{436}$) and UV-absorbing centers (UV_{365} and UV_{254}) as described elsewhere (Uyguner and Bekbolet 2005a, b; Uyguner-Demirel and Bekbolet 2011). Besides, the application of UV–vis absorbance ratios (A_{254}/A_{436}, A_{280}/A_{436}, A_{254}/A_{365}, A_{280}/A_{365}, and A_{253}/A_{203} UV_{250}/UV_{365}) could imply the removal of color forming groups in correlation to the removal of UV-absorbing centers revealing spectral variations of RfOM (Uyguner and Bekbolet 2005a, b).

Fluorescence spectroscopic parameters A Perkin Elmer LS 55 Luminescence Spectrometer equipped with a 150 W xenon arc lamp and a red sensitive photomultiplier tube was used for the characterization of fluorescence features in synchronous scan mode. Synchronous scan was acquired in the excitation wavelength range of 200–600 nm ($\Delta\lambda = 18$ nm).

Dissolved organic carbon A Shimadzu Vwp TOC analyzer was used for the determination of DOC (mg L^{-1}) in non-purgeable organic carbon mode.

Following each treatment period, photocatalyst was immediately removed from the reaction medium via double filtration through 0.45 µm and 0.22 µm membrane filters to avoid post-adsorption of organics onto photocatalyst specimens.

Results and discussion

Due to the possibility of various reactions prevailing between components and to understand the interactions in the aqueous medium, mono- and binary systems were defined as follows:

1. Interactions under irradiation; (i) light and sole RfOM revealing direct photolysis of the substrate to be described by spectral features, (ii) light and sole PANI specimens expressing stability under irradiation followed by spectral analysis, (iii) light and "RfOM and photocatalyst specimens" indicating photocatalysis described by spectral analysis, respective parameters as well as kinetic modeling.
2. Interactions under dark conditions: (i) sole PANI specimens expressing stability under dark conditions followed by spectral analysis, (ii) RfOM adsorption onto all photocatalyst specimens revealing surface interactions followed by spectral features.

Preliminary experiments of RfOM and PANI under simulated solar irradiation

UV–vis and fluorescence spectra of RfOM displayed similar pattern to that of HA as verified by respective parameters under all experimental conditions. The photochemistry of RfOM, i.e., humic matter is complicated due to ill-defined structure of the material (Loiselle et al. 2012). Characterization of photolysis products is hindered by the limitations of humic chemistry giving no way to identification of an exact molecular structure. Hence, integrative data and sum parameters of UV–vis and fluorescence spectroscopy have been used for description of humic educts and products, as well as for the chromophores (Frimmel 1990; Korshin et al. 1999).

It is very well documented that in aquatic systems, RfOM acts both as a photosensitizer and a quencher. The photosensitizing properties are due to production of triplet RfOM (^{3}RfOM) and reactive oxygen species (ROS, i.e., $O_2^{\bullet-}$, $HO^{\bullet}$, and H_2O_2) along with excited state of RfOM* (Eqs. 1–11) (Dalrymple et al. 2010).

$$^1\mathrm{RfOM} + \mathrm{hv} \rightarrow {}^1\mathrm{RfOM}* \rightarrow \text{intersystem crossing} \rightarrow {}^3\mathrm{RfOM}* \quad (1)$$

$$^3\mathrm{RfOM}* \rightarrow {}^1\mathrm{RfOM} + {}^1\mathrm{O_2} \quad (2)$$

$$^1\mathrm{RfOM} + \mathrm{hv} \rightarrow \mathrm{RfOM}^{\bullet+/\bullet-} \quad (3)$$

$$^1\mathrm{RfOM}* \rightarrow \mathrm{RfOM}^{\bullet+/\bullet-} \quad (4)$$

$$^3\mathrm{RfOM}* \rightarrow \mathrm{RfOM}^{\bullet+/\bullet-} \quad (5)$$

$$\mathrm{RfOM}^{\bullet+/\bullet-} + \mathrm{O_2} \rightarrow^{\bullet} \mathrm{RfOM}^{+} + \mathrm{O_2}^{-} \quad (6)$$

$$^3\mathrm{RfOM}* + \mathrm{O_2} \rightarrow^{\bullet} \mathrm{RfOM}^{+} + \mathrm{O_2}^{-} \quad (7)$$

$$^1\mathrm{RfOM} + {}^1\mathrm{O_2} \rightarrow \mathrm{O_2}^{-} +^{\bullet} \mathrm{RfOM}^{+} \rightarrow \text{products} \quad (8)$$

$$^3\mathrm{RfOM}* + \mathrm{H_2O} \rightarrow \mathrm{RfOM} - \mathrm{H}^{\bullet} + \mathrm{HO}^{\bullet} \quad (9)$$

$$^3\mathrm{RfOM}* + \mathrm{O_2} \rightarrow (\mathrm{RfOM})_{\mathrm{deg}} + \mathrm{O_2}^{\bullet-}/\mathrm{HO_2}^{\bullet} \quad (10)$$

$$^3\mathrm{RfOM}* + \mathrm{O_2} \rightarrow {}^1\mathrm{RfOM} + {}^1\mathrm{O_2} \quad (11)$$

Following the formation of oxygen radicals, several consecutive (Eqs. 12–16) as well as radical termination (Eqs. 17–19) reactions would also take place.

$$\mathrm{O_2}^{\bullet-}/\mathrm{HO_2}^{\bullet} \rightarrow \mathrm{H_2O_2} \quad (12)$$

$$2\mathrm{O_2}^{\bullet-} + 2\mathrm{H}^{+} \rightarrow \mathrm{H_2O_2} + \mathrm{O_2} \quad (13)$$

$$\mathrm{H_2O_2} \leftrightarrow \mathrm{H}^{+} + \mathrm{HO_{2^-}} \quad \mathrm{pK_a} = 11.6 \quad (14)$$

$$2\mathrm{O_2}^{\bullet-} + \mathrm{H_2O_2} \rightarrow \mathrm{O_2} + \mathrm{HO}^{\bullet} + \mathrm{OH}^{-} \quad (15)$$

$$\mathrm{O_2}^{\bullet-} + \mathrm{H}^{+} \rightarrow \mathrm{HO_2}^{\bullet} \quad (16)$$

$$\mathrm{O_2}^{\bullet-} + \mathrm{HO_2}^{\bullet} \rightarrow \mathrm{HO_{2^-}} + \mathrm{O_2} \quad (17)$$

$$\mathrm{HO_2}\cdot + \mathrm{HO_2}\cdot \rightarrow \mathrm{O_2} + \mathrm{H_2O_2} \quad (18)$$

$$\mathrm{HO}^{\bullet} + \mathrm{HO_2}^{\bullet} \rightarrow \mathrm{H_2O} + \mathrm{O_2} \quad (19)$$

Species present in RfOM-based radical pool react either through a non-selective route ($HO^{\bullet}$, $E^{\circ} = 2.80$ V) or via selective reaction pathways (e.g., $^1O_2$, $E^{\circ} = 1.10$ V) with the compounds present in vicinity of the source. Furthermore, these species could selectively target electron-rich moieties such as phenols and/or activated aromatics (Lee and von Gunten 2010). In the presence of organic matter under simulated sunlight, formation of $^1O_2$ and H_2O_2 was also reported as contributing to the reaction medium (Garg et al. 2011). Based on this reaction mechanism, direct phototransformation was predicted along with insignificant self-degradation of RfOM (< 5%). Furthermore, sensitizing effect was expected in the presence of PANI and PANI-TiO_2 specimens upon irradiation during photocatalysis.

Sole PANI specimen (0.25 mg mL^{-1}) in distilled water was also exposed to simulated solar irradiation

(t_{irr} = 120 min) and expressed considerable stability as confirmed by UV–vis spectral analysis of the released organic matrix. Similarly, under dark conditions, sole PANI exhibiting similar declining feature also revealed very low absorptivity.

Adsorptive interactions in the absence of light

Adsorption of the substrate at the surface of the photocatalyst is a critical step that determines the interaction of induced ROS with the substrate. Initial adsorption, i.e., t = 0 min condition represented the instantaneous introduction of the photocatalyst particle to RFOM solution and its subsequent removal by filtration through 0.45 µm membrane filter. Surface interactions could be visualized as governed by simultaneously operating attractive and repulsive forces between deprotonated functional groups of the adsorbate (macromolecular organic oxyanion size fractions) and photocatalyst surface acquiring both charges (Turkten et al. 2019).

As a basis for comparison, TiO_2 displayed a decreasing order of color forming chromophoric moieties followed by UV-absorbing centers ($Color_{436} > UV_{365} > UV_{254} > UV_{280}$). The reason was extensively explained in terms of pH dependent electrostatic attractions in relation to surface charge development on the oxide surface (pH_{zpc} = 6.3) as well as the deprotonated carboxylic functional groups of humic acid (Uyguner and Bekbolet 2005a).

Highest initial adsorption extents were attained in the presence of sole PANI ($UV_{280} > UV_{254} > UV_{365} > Color_{436}$) in accordance with recent literature findings showing that PANI is effective for adsorbing HA (Wang et al. 2014). The order of removal of RfOM in the presence of PANI indicated that the dense aromatic structures played the major role in hydrophobic attractions even van der Waal's forces. Humic molecules are known to be negatively charged due to deprotonation of carboxylic and phenolic groups at a wide range of pH (2–10) (Baglieri et al. 2014) while PANI having imine (–NH^+–) and amine (–NH_2–) groups are cationic over this pH range (Laabd et al. 2016; Wang et al. 2012, 2015). Hence, electrostatic attraction was expected to contribute to better removal efficiencies as presented in Fig. 1. Considering the presence of charged moieties in humic structure, interactions between polar functional groups of the adsorbate (i.e., carboxylate functions) and the nitrogen heteroatom of PANI are plausible.

Considering PANI-TiO_2 composites, incorporation of PANI to TiO_2 affected the extent of dark interactions as displayed by all UV–vis parameters. With a decrease in PANI content, the adsorption capacity of composites also decreased although relatively close removal percentages were attained for PT-14 and PT-18. Competing role of both color forming moieties and UV-absorbing centers

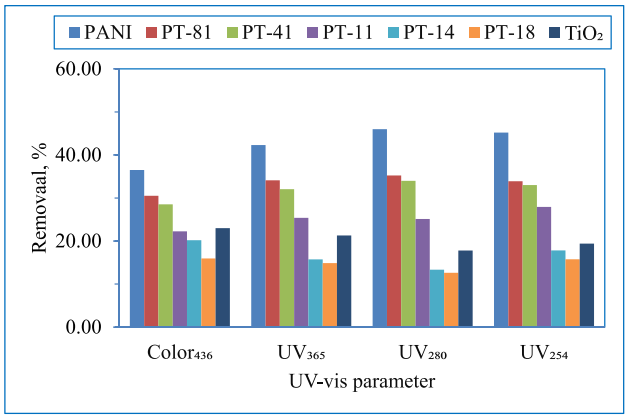

Fig. 1 t = 0 condition, removal of UV–vis spectroscopic parameters by initial adsorption

representing deprotonated functional groups and lone pair electron centers of conjugated systems versus dense aromatic skeleton expressing mainly hydrophobic character should be considered. As a general trend, UV-absorbing centers were relatively better adsorbed than color-forming moieties. It could also be deduced that the role of UV-absorbing centers predominated over surface area effect during dark interactions. Based on UV_{254} data, the adsorption extent of RfOM onto sole PANI was 45.20% whereas incorporation of PANI into TiO_2 structure, e.g., PT-11 expressed 27.92% removal in comparison to sole TiO_2 as 19.40%.

FT-IR features of the initial adsorption conditions of PANI and PANI-TiO_2 in the presence of RfOM were documented in detail as reported in manuscript, Part I (Turkten et al. submitted for publication). Slight shifts in the peak positions were observed due to the adsorption of RfOM. The reason could be the electron transfers pertaining between PANI and TiO_2 (Sarmah and Kumar 2011). Moreover, the peak related to surface anions of the protonated part of PANI at 575 cm^{-1} vanished with increasing TiO_2 concentration (PT-11, PT-14 and PT-18). UV-absorbing centers as presented in Fig. 1 were consistent with this finding and the presence of surface anions of PANI could play a remarkable role on the interactions of charged moieties on RfOM.

The surface characteristic properties of PANI, TiO_2, and PT-11 are presented in SM, Table SM1. The high adsorption capacity was related to high surface area and pore volume. Surface area displaying a significant role in dark interactions of the complex adsorbate/adsorbent system indicated an inconsistent effect with respect to both specimen and organic matrix conditions. BET surface areas of PT-11, PANI and TiO_2 were 34.3 $m^2\ g^{-1}$, 26.1 $m^2\ g^{-1}$, and 55 $m^2\ g^{-1}$, respectively, indicating an inverse relationship with initial adsorption profiles. Modifying TiO_2 with PANI led to a decrease in surface area of the composite probably hindering electrostatic interactions. Wang and colleagues reported lower

surface areas for PANI/TiO_2, TiO_2, and PANI specimens as 11.894, 5.235, and 19.214 $m^2\ g^{-1}$, respectively (Wang et al. 2019). On the other hand, Zhang and colleagues reported no significant change in the surface area of TiO_2 (50.1 $m^2\ g^{-1}$) and PANI modified TiO_2 (49.7 $m^2\ g^{-1}$) (Zhang et al. 2008). The difference could be attributed to the preparation methodology of PANI/TiO_2 specimens resulting in inconsistent comparisons.

Furthermore, selected absorbance quotients as A_{254}/A_{436}, A_{280}/A_{436}, A_{254}/A_{365}, A_{280}/A_{365}, and A_{253}/A_{203} were also presented (Fig. 2). The absorbance quotient A_{250}/A_{365} which describes a shift towards absorption in the red part of the spectrum, was positively correlated with low-molecular-weight DOC compounds while negatively related to average molecular DOC weight (Berggren et al. 2010; Dahlén et al. 1996; Uyguner and Bekbolet 2005b). Therefore, A_{254}/A_{365} was chosen as a simple index indicating the possible diversity of heterogeneous organic matrix (Ågren et al. 2008).

Insignificant variations of A_{254}/A_{365} quotient were attained under all conditions. Similarly, A_{280}/A_{365} quotients were also almost invariable for all photocatalyst specimens. On the other hand, A_{254}/A_{436} and A_{280}/A_{436} quotients exhibited a variable trend, while lowest values were observed in the presence of sole PANI. Hence, neither A_{254}/A_{365} nor A_{280}/A_{365} could be recognized as indicative parameters. A plausible explanation could be related to the contribution of color forming moieties rather than the aromatic core with respect to photocatalyst type. Since all UV–vis parameters represented the humic structure comprised of conjugated double bond systems and a dense aromatic core, both electrostatic and hydrophobic interactions should be considered. Sun and colleagues investigated the adsorptive interactions of PANI and tannic acid composition which highly resembled humic macromolecules (Sun et al. 2017). In their study, mechanism of adsorption was explained with the mutual roles of van der Waal's forces, π–π interactions and hydrogen bonding prevailing between PANI chains and organic fractions.

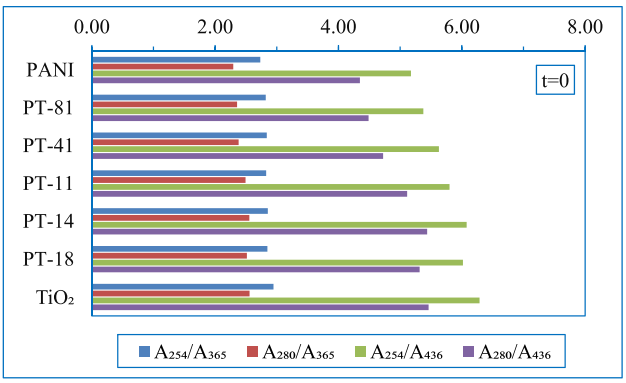

Fig. 2 $t=0$ condition, selected absorbance quotient profiles upon initial adsorption

It should also be emphasized that two opposing phenomena could be visualized: (i) TiO_2 surface could be deposited by PANI emeraldine salt avoiding TiO_2 agglomeration due to the presence of positive charges excluding each other (Li et al. 2008); (ii) TiO_2 particles could also be deposited onto PANI chains (Gu et al. 2012). Furthermore, the effect of PANI coating onto TiO_2 particle could shield direct light harvesting of TiO_2 enabling indirect e^- injection from sensitized PANI to TiO_2.

Under these conditions, inconsistent descriptions are available in literature on the morphology of PANI/HA by TEM images with differing magnifications. Zhang and colleagues reported that PANI/HA particles exhibited spherical shape with an average size of 50–60 nm whereas Li and co-workers defined a complex network structure with sizes about 10–20 nm (Li et al. 2011; Zhang et al. 2010).

Photocatalytic degradation of RfOM using PT specimens

Fundamentally, upon irradiation with UV/visible light, semiconductors catalyze redox reactions in the presence of air/O_2 and water. Through the formation of reactive oxygen and radical species degradation/decomposition reactions take place (Banerjee et al. 2006). Considering the most versatile photocatalyst TiO_2, in aqueous phase, primary events followed by reactions taking place in the presence of O_2 are given as follows (Eqs. 20–31):

$$TiO_2 + hv\left(E \geq E_{bg}\right) \rightarrow TiO_{2,CB}, e^- + TiO_{2,VB}h^+) \quad (20)$$

Reactions involving $TiO_{2,CB}$,e^-

$$TiO_{2,CB,}e^- + O_2 \rightarrow TiO_2 + O_2^{\bullet -} \quad (21)$$

$$TiO_{2,CB,}e^- + O_2^{\bullet -} + 2H^+ \rightarrow TiO_2 + H_2O_2 \quad (22)$$

$$TiO_{2,CB,}e^- + H_2O_2 \rightarrow TiO_2 + HO^{\bullet} + OH^- \quad (23)$$

$$2O_2^{\bullet -} + H_2O_2 \rightarrow HO^{\bullet} + OH^- + O_2 \quad (24)$$

$$O_2^{\bullet -} + H^+ \rightarrow HO_2^{\bullet} \quad (25)$$

$$TiO_{2,CB,}e^- + HO_2^{\bullet} \rightarrow TiO_2 + HO_{2-} \quad (26)$$

$$HO_{2-} + H^+ \rightarrow H_2O_2 \quad (27)$$

$$HO_2^{\bullet} + HO_2^{\bullet} \rightarrow O_2 + H_2O_2 \quad (28)$$

Reactions involving $TiO_{2,VB,}h^+$

$$TiO_{2,VB,}h^+ + H_2O_{ads} \rightarrow TiO_2 + HO^{\bullet}{}_{ads} + H^+ \quad (29)$$

$$TiO_{2,VB,}h^+ + H_2O_{ads} \rightarrow TiO_2 + H_2O_2 + H^+ \quad (30)$$

$$TiO_{2,VB,}h^+ + OH^- \rightarrow TiO_2 + HO^{\bullet}{}_{ads} \quad (31)$$

Radical termination reactions could also take place forming mainly H_2O_2 and O_2 (Eqs. 17–19).

Upon visible light irradiation charge separation would take place due to energy difference (E = 2.8 eV) between HOMO and LUMO levels of PANI (Jangid et al. 2021; Li et al. 2008; Zhang et al. 2008). Excluding recombination of back-reaction in the presence of TiO_2 expressing wider band gap, promoted electrons could be injected to the conduction band of TiO_2. These electrons could possibly take role in aforementioned reactions, and the photogenerated holes of TiO_2 would also react as expected (Eqs. 32–35).

$$PANI/TiO_2 + hv \rightarrow PANI^+/TiO_2 + e^-{}_{CB} \quad (32)$$

$$e^-{}_{CB} + O_2 \rightarrow O_2^{\bullet -} \quad (33)$$

$$PANI^+/TiO_2 \rightarrow PANI/TiO_2 + h^+{}_{VB} \quad (34)$$

$$h^+{}_{VB} + \left(H_2O \leftrightarrow H^+ + OH^-\right) \rightarrow H^+ + HO^{\bullet} \quad (35)$$

$PANI/TiO_2$ nanocomposites could be activated simultaneously by UV and visible light. Under UV-irradiation, both PANI and TiO_2 could absorb photons and via e^- reactions with O_2 superoxide radicals and further reactions with H_2O, $HO^{\bullet}$ radicals could form. Moreover, upon absorption of visible light ($\lambda > 400$ nm) by $PANI/TiO_2$, the transitions $\pi \rightarrow$ polaron and polaron $\rightarrow \pi^*$ in PANI molecules could be expected. Excited-state electrons from PANI molecules could be injected to $TiO_{2,CB}$ and through reaction with $O_{2,ads}$ ROS would be formed. The photogenerated PANI, h^+ migrating to the interface could form hydroxyl radicals via reactions with H_2O. Therefore, under simulated solar light conditions, generation of $HO^{\bullet}$ radicals as well as ROS could be explained. Thus, PANI could serve as a sensitizer, an efficient electron donor and also as a good hole transporter (Yang et al. 2017). Based on the formation and reactivity of ROS attained via sole TiO_2 photocatalysis (Eqs. 20–31) in combination with the sensitizing effect of PANI leading to complex intra-system ROS formation in PANI-TiO_2 composite (Eqs. 32–35), degradation of RfOM could be accomplished. It should also be emphasized that under solar irradiation humic moieties could also act as photosensitizers resulting in double synergy of photosensitization effect.

Under the specified reaction conditions, photocatalytic progression was monitored by spectral features of RfOM during light exposure of 0–120 min in certain intervals using all photocatalysts, i.e., PANI, TiO_2, and PT specimens. UV–vis spectral features revealed that RfOM retained characteristic logarithmic decreasing profiles upon use of all photocatalyst specimens including sole PANI as presented in SM in Fig. SM2.

The absorption of visible light would increase as PANI/TiO_2 ratio increased in favor of PANI (PT-11, PT-41, and PT-81) due to the light harvesting capacity of both PANI and RfOM, which was beneficial for ROS generation. Contrary to this case, absorption of light decreased as PANI/TiO_2 ratio (PT-11, PT-14, and PT-18) changed in favor of TiO_2 due to the obstructive effect from excess TiO_2, which was detrimental for the generation of ROS. Incremental contribution of PANI to TiO_2 exerted an irradiation time dependent variable effect that was more pronounced for PT-18 resembling sole TiO_2.

Variations in selected absorbance quotients as A_{254}/A_{436}, A_{280}/A_{436}, A_{254}/A_{365}, A_{280}/A_{365}, and A_{253}/A_{203} were also compared with respect to irradiation time and photocatalyst type (Fig. SM3). As already stated, A_{254}/A_{436} was evaluated as depicted in Fig. 3. From a general perspective, irradiation time-dependent specimen-specific discrepancies were observed. Sole PANI expressed a slightly decreasing trend whereas sole TiO_2 displayed a dramatic decrease following 20 min of exposure then showing a similar trend to sole PANI. However, under $t = 0$ condition that represented the role of UV-absorbing centers to color forming moieties in adsorption, the following trend was achieved for A_{254}/A_{436}; $TiO_2 >$ PT-14 > PT-18 > PT-11 > PT-41 > PT-81 > PANI (Fig. 2).

During photocatalysis, almost all absorbance quotients increased compared to $t = 0$ condition, although substantial losses were attained in DOC contents. Therefore, a correlative approach was presented relating absorbance quotients,

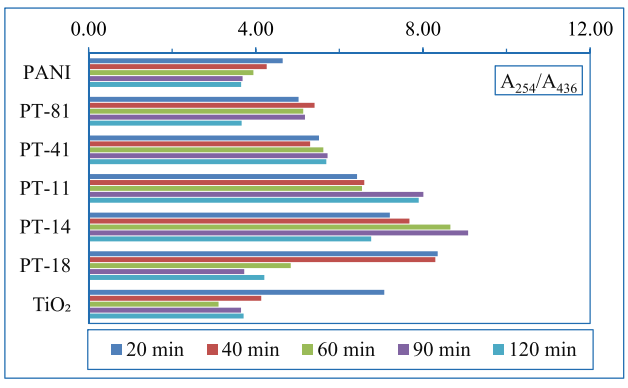

Fig. 3 Irradiation time (min) dependent variations of A_{254}/A_{436} during photocatalysis

i.e., A_{254}/A_{436}, A_{280}/A_{436}, A_{254}/A_{365}, A_{280}/A_{365} as well as A_{253}/A_{203} to the removal of DOC contents (Fig. 4a–g). Upon use of sole TiO_2, A_{253}/A_{203} quotient displayed a decreasing trend as 0.78–0.23 representing the presence of high molecular weight organic fractions composed of aromatic rings along with DOC removal up to 85% (~1 mg L^{-1}). All other absorbance quotients showed fluctuations indicating the balancing role of color-forming moieties and UV-absorbing centers. In the presence of PT-11, a rather steady decreasing profile was attained for A_{253}/A_{203} quotient. The incorporation effect of PANI into TiO_2 composite could be visualized in A_{280}/A_{365} and A_{254}/A_{365} quotients exhibiting an almost constant and parallel trend. Upon use of PT-14, a rather steady decreasing profile was attained for A_{253}/A_{203} quotient as 0.76–0.61 followed by a dramatic decrease down to 0.19 in 120 min. The incorporation effect of PANI into TiO_2 composite could also be visualized in A_{280}/A_{365} and A_{254}/A_{365} quotients. Furthermore, upon use of PT-18, a rather similar profile to PT-14 was observed in A_{280}/A_{365} and A_{254}/A_{365} quotients. On the other hand, a different profile was remarkable upon use of PT-41, expressing an almost insignificant change irrespective of DOC removals. The incorporation of PANI in higher ratios into TiO_2 drastically affected the quotient distribution in a no-changing linear trend. Although 64% DOC was removed, A_{253}/A_{203} quotient was still 0.54 representing almost similar organic consortium. Inspecting data for PT-81, a similar profile to PT-41 was observed expressing an almost insignificant change irrespective of DOC removals. The incorporation of PANI in 8:1 ratio into TiO_2 drastically affected the quotient distribution in a linear trend following 35% DOC removal while A_{253}/A_{203} quotient was 0.52 representing almost similar spectroscopic properties as that of PT-41. However, in the presence of PANI, all quotients displayed a steady decreasing profile irrespective of DOC removals indicating the role of all components upon irradiation. A_{253}/A_{203} quotient ranged from 0.78 to 0.47 while 88% removal in DOC was attained in 120 min of photocatalytic oxidation.

Synchronous fluorescence spectra could bring in resolved information about the organic matrix composition (Senesi 1990; Senesi et al. 1991). As reported previously, FI_{syn} (λ_{emis} = 200–600 nm) displayed the presence of major fluorophoric region and shifts to lower wavelengths during photocatalysis (Uyguner and Bekbolet 2005a) (Fig. SM4). The major fluorophoric region centered at λ_{emis} ~ 470 nm and designated as $FI_{syn,470}$ expressed variations with respect to irradiation time (Fig. SM5). As a general trend, decrease in fluorescence intensity is expected with photocatalysis under extended irradiation conditions, however, an abrupt

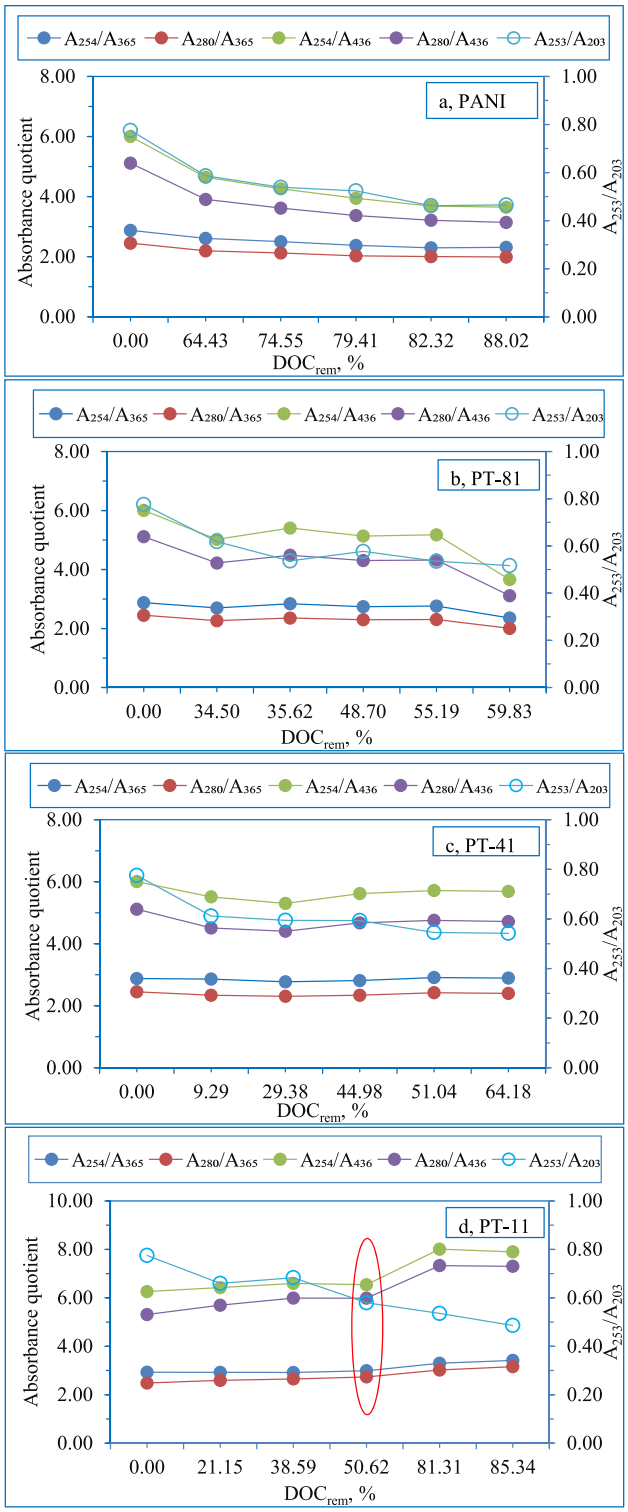

Fig. 4 **a–g** Absorbance quotients with respect to DOC removals, % upon use of all photocatalyst specimens

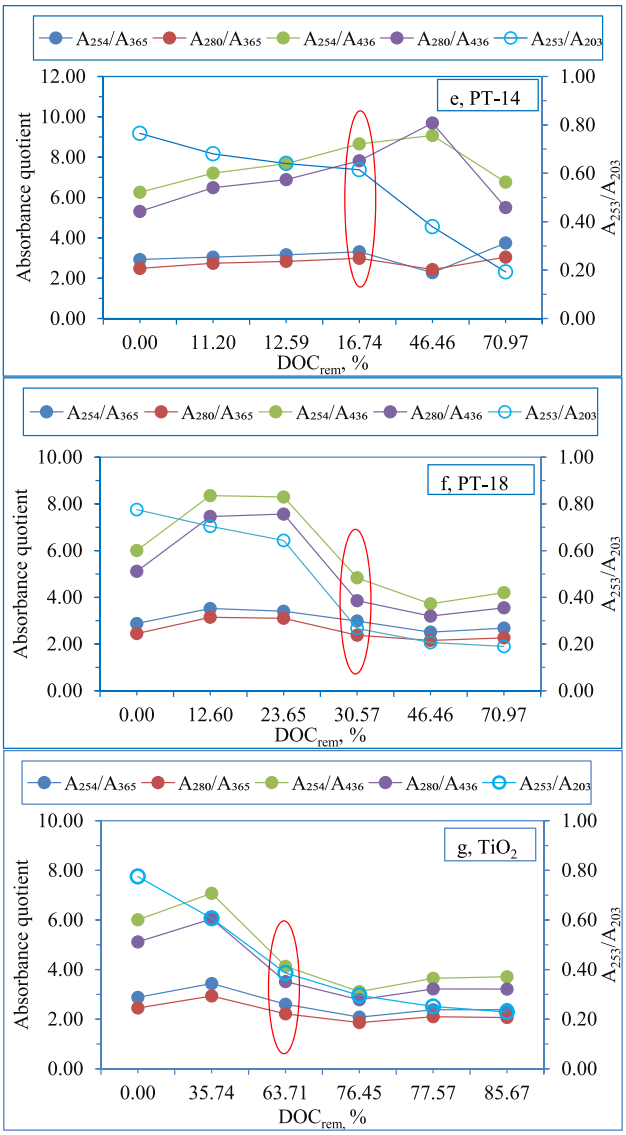

Fig. 4 (continued)

decline in the presence of PT-14 and PT-18 is noteworthy. In accordance with high removal rates, destruction of aromatic moieties could be deduced from fluorescence intensities. Contrary to other photocatalyst specimens, PT-11 exhibits high FI_{syn} values at 90 min and 120 min. Synchronous fluorescence spectral features and observed variations to lower wavelengths could be explained by utilization of these fluorophores during photocatalysis as well as during primary adsorptive interactions (Uyguner and Bekbolet 2005a).

Kinetics of photocatalytic degradation

As evidenced by spectral features (Fig. SM2), all UV–vis parameters obeyed pseudo-first-order kinetic model (Eq. 36).

Table 1 Photocatalytic degradation kinetics of RfOM expressed by the specified UV–vis parameters

Kinetics	UV–vis spectroscopic parameters			
PANI	$Color_{436}$	UV_{365}	UV_{280}	UV_{254}
$kx10^{-2}$, min	0.923	1.123	1.279	1.300
Rate, cm^{-1} min^{-1}	0.00121	0.00307	0.00857	0.01023
$t_{1/2}$, min	75.1	61.7	54.2	53.3
PT-81				
$kx10^{-2}$, min	0.547	0.730	0.852	0.852
Rate, cm^{-1} min^{-1}	0.00072	0.00200	0.00571	0.00671
$t_{1/2}$, min	126.7	95.0	81.4	81.4
PT-41				
$kx10^{-2}$, min	0.971	0.992	0.987	0.978
Rate, cm^{-1} min^{-1}	0.00127	0.00271	0.00662	0.00770
$t_{1/2}$, min	71.4	69.9	70.2	70.9
PT-11				
$kx10^{-2}$, min	1.490	1.411	1.206	1.266
Rate, cm^{-1} min^{-1}	0.00194	0.00393	0.00834	0.01032
$t_{1/2}$, min	46.5	49.1	57.5	54.8
PT-14				
$kx10^{-2}$, min	2.093	2.750	2.337	2.271
Rate, cm^{-1} min^{-1}	0.00273	0.00766	0.01617	0.01852
$t_{1/2}$, min	33.1	25.2	29.7	30.5
PT-18				
$kx10^{-2}$, min	1.613	2.001	2.220	2.190
Rate, cm^{-1} min^{-1}	0.00211	0.00547	0.01488	0.01724
$t_{1/2}$, min	43	34.6	31.2	31.6
TiO_2				
$kx10^{-2}$, min	1.177	1.448	1.675	1.701
Rate, cm^{-1} min^{-1}	0.00154	0.00396	0.01123	0.01339
$t_{1/2}$, min	58.9	47.9	41.4	40.7

$$\text{Rate (R)} = -dA/dt = kA \tag{36}$$

where

R pseudo-first-order rate (cm^{-1} min^{-1})
A_o initial absorbance of RfOM UV–vis parameters
A absorbance of RfOM at time t

t irradiation time, min
k pseudo-first-order reaction rate constant, min^{-1}

Half-life ($t_{1/2}$, min) could easily be calculated by the following equation, $t_{1/2} = 0.693/k$

Kinetic model parameters ($R^2 > 0.85$) are presented in Table 1.

For all UV–vis parameters analyzed, the highest and lowest rate constants were attained in the presence of PT-14 and PT-81, respectively. Moreover, half-life values ($t_{1/2}$, min) ranged from 40.7 to 58.9 min in the presence of

TiO_2, while values in the range of 81.4 to 126.7 min were attained in case of PT-81. Wang and colleagues reported the isoelectric points of PANI, TiO_2, and PANI/TiO_2 as 7.05, 2.66, and 5.2, respectively (Wang et al. 2019). The band gap energies (E_{bg}) for TiO_2 and TiO_2/PANI determined by using Tauc plot via modified Kubelka–Munk function with linear extrapolation were presented as 3.17 and 2.88 eV (Asgari et al. 2019). Moreover, Lee and co-workers reported that E_{bg} of pristine TiO_2 and PANI/TiO_2 composites were 3.21 and 3.15 eV, respectively. A similar reduction in band gap energy of PANI/TiO_2 composite (3.07 eV) has also been revealed in some studies, which could lead to higher photocatalytic activity (Lee et al. 2020; Li et al. 2008). Efficient shifting of the photoresponse of TiO_2 to visible range after polyaniline incorporation has been confirmed by band-gap energies as 2.71 eV, 2.82 eV, 2.90 eV, 2.96 eV, 3.06 eV, and 3.20 eV for PT-81, PT-41, PT-11, PT-14, PT-18, and TiO_2, respectively (Turkten et al. 2023). The bandgap energies directly indicated the effective utilization of solar irradiation leading to degradation of organic matter.

On the other hand, the effect of initial adsorption extent of RfOM onto PANI as expressed by all UV–vis parameters could not be directly correlated with degradation rate profiles. Although the lowest surface interactions were attained for PT-14 and PT-18, considerable enhancement in photocatalytic activity was observed for these PANI-TiO_2 composites compared to pure TiO_2 for the degradation of RfOM in terms of all defined UV–vis parameters (Fig. 5). The surface charge of the PANI/TiO_2 composites could be expected at pH 5–6 with respect to pertaining components as PANI ($pH_{zpc} = 5.8$) and TiO_2 ($pH_{zpc} = 6.3$) (Birben et al. 2017; Wang et al. 2009). Therefore, surface interactions leading to differing adsorption extents could not be simply attributed to the electrostatic interactions but could be related to coincidental interactions due to hydrophobic/hydrophilic character of humic sub-fractions under stirring conditions.

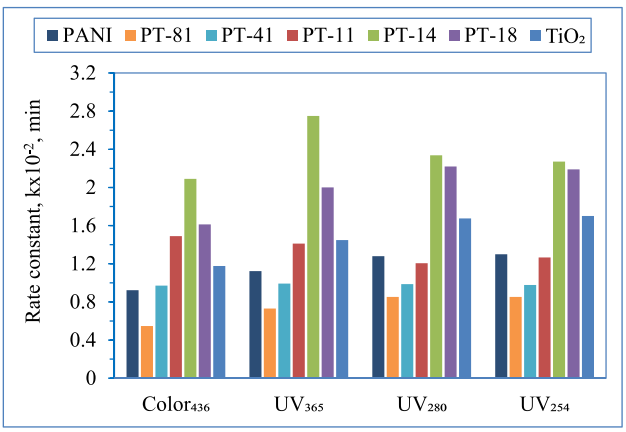

Fig. 5 Rate constants of photocatalytic degradation of RfOM expressed by the specified UV–vis spectroscopic parameters upon use of all photocatalyst specimens

Conclusions

PANI has been regarded as a promising conducting polymer. To overcome the inherent drawbacks of TiO_2, a strategic combination of PANI and TiO_2 was accomplished in this study by in-situ chemical oxidation polymerization method to provide better stability and conductivity, as well as enhanced photocatalytic performance. Despite its practical properties, a limited number of studies has been carried out to degrade organic pollutants by TiO_2 modified PANI. To extend research on the use of modified photocatalysts for the elimination of organic matter that has adverse effects on drinking water quality, a comparative work was presented to test their activity for the removal of RfOM under simulated solar irradiation. Among all PANI-TiO_2 composites with different mole ratios, noteworthy enhancement in photocatalytic activity was achieved in the presence of PT-14 and PT-18 compared to pristine TiO_2 in terms of all defined UV–vis parameters. Kinetic data confirmed the highest rate constants for PT-14 (2.093×10^{-2} to 2.750×10^{-2} min^{-1}) and lowest rate constants for PT-81 (5.47×10^{-3} to 8.52×10^{-3} min^{-1}). The results highlight the applicability of PANI-TiO_2 for the removal of recalcitrant organic compounds. The synergetic effect between PANI and TiO_2 was more pronounced in lower PANI ratios whereas higher PANI ratios reflected a retardation effect up to a specific mass ratio of polyaniline to TiO_2. Further investigation of optimum dosages would still be required for practical applications. It could be concluded that PANI-TiO_2 composite with enhanced visible-light photocatalytic efficiency and stability can be utilized for the degradation of contaminants in water treatment. Moreover, a thorough investigation and assessment of spectroscopic parameters of UV–vis and fluorescence can also provide a proxy for practical applications in control and rapid estimation of RfOM in water treatment.

Supplementary Information The online version contains supplementary material available at https://doi.org/10.1007/s11356-023-28385-0.

Author contribution Material characterization tests were performed by both Nazli Turkten and Yunus Karatas. Photocatalytic experiments and analysis were carried out by Nazli Turkten. Miray Bekbolet, Nazli Turkten, and Ceyda S. Uyguner-Demirel contributed to the study conceptualization and design. Data analysis, evaluation, writing, and editing of the manuscript was realized by Ceyda S. Uyguner-Demirel and Miray Bekbolet.

Data availability The data that support the findings of this study are available from the authors upon reasonable request.

Declarations

Ethics approval Not applicable.

Consent to participate Not applicable.

Consent for publication The submission is original, not under consideration for publication elsewhere, and that all authors are aware of the submission and agree to its publication.

Competing interests The authors declare no competing interests to.

References

Ågren A, Berggren M, Laudon H, Jansson M (2008) Terrestrial export of highly bioavailable carbon from small boreal catchments in spring floods. Freshw Biol 53:964–972. https://doi.org/10.1111/j.1365-2427.2008.01955.x

Asgari E, Esrafili A, Jonidi Jafari A, Rezaei Kalantary R, Farzadkia M (2019) Synthesis of TiO_2/polyaniline photocatalytic nanocomposite and its effects on degradation of metronidazole in aqueous solutions under UV and visible light radiation. Desalination Water Treat 161:228–242. https://doi.org/10.5004/dwt.2019.24291

Baglieri A, Vindrola D, Gennari M, Negre M (2014) Chemical and spectroscopic characterization of insoluble and soluble humic acid fractions at different pH values. Chem Biol Technol Agric 1:9. https://doi.org/10.1186/s40538-014-0009-x

Banerjee S, Gopal J, Muraleedharan P, Tyagi AK, Raj B (2006) Physics and chemistry of photocatalytic titanium dioxide: visualization of bactericidal activity using atomic force microscopy. Curr Sci 90:1378–1383. https://www.jstor.org/stable/24091987

Berggren M, Laudon H, Haei M, Ström L, Jansson M (2010) Efficient aquatic bacterial metabolism of dissolved low-molecular-weight compounds from terrestrial sources. ISME J 4:408–416. https://doi.org/10.1038/ismej.2009.120

Birben NC, Uyguner-Demirel CS, Kavurmaci SS, Gürkan YY, Turkten N, Cinar Z, Bekbolet M (2017) Application of Fe-doped TiO_2 specimens for the solar photocatalytic degradation of humic acid. Catal Today 281:78–84. https://doi.org/10.1016/j.cattod.2016.06.020

Cui W, He J, Wang H, Hu J, Liu L, Liang Y (2018) Polyaniline hybridization promotes photo-electro-catalytic removal of organic contaminants over 3D network structure of rGH-PANI/TiO_2 hydrogel. Appl Catal B 232:232–245. https://doi.org/10.1016/j.apcatb.2018.03.069

Dahlén J, Bertilsson S, Pettersson C (1996) Effects of UV-A irradiation on dissolved organic matter in humic surface waters. Environ Int 22:501–506. https://doi.org/10.1016/0160-4120(96)00038-4

Dalrymple RM, Carfagno AK, Sharpless CM (2010) Correlations between dissolved organic matter optical properties and quantum yields of singlet oxygen and hydrogen peroxide. Environ Sci Technol 44:5824–5829. https://doi.org/10.1021/es101005u

Deng Y, Tang L, Zeng G, Dong H, Yan M, Wang J, Hu W, Wang J, Zhou Y, Tang J (2016) Enhanced visible light photocatalytic performance of polyaniline modified mesoporous single crystal TiO_2 microsphere. Appl Surf Sci 387:882–893. https://doi.org/10.1016/j.apsusc.2016.07.026

Doğan D, Taş R, Can M (2020) Increasing photocatalytic stability and photocatalytic property of polyaniline conductive polymer. Iran J Sci Technol Trans a: Sci 44:1025–1037. https://doi.org/10.1007/s40995-020-00922-3

Drosos M, Ren M, Frimmel FH (2015) The effect of NOM to TiO_2: interactions and photocatalytic behavior. Appl Catal B 165:328–334. https://doi.org/10.1016/j.apcatb.2014.10.017

Eskizeybek V, Sarı F, Gülce H, Gülce A, Avcı A (2012) Preparation of the new polyaniline/ZnO nanocomposite and its photocatalytic activity for degradation of methylene blue and malachite green dyes under UV and natural sun lights irradiations. Appl Catal B 119–120:197–206. https://doi.org/10.1016/j.apcatb.2012.02.034

Feng H, Liang YN, Hu X (2022) Natural organic matter (NOM), an underexplored resource for environmental conservation and remediation. Mater Today Sustain 19:100159. https://doi.org/10.1016/j.mtsust.2022.100159

Frimmel FH (1990) Organic acids in aquatic ecosystems. In: Perdue EM, Gjessing ET (eds) Characterization of organic acids in freshwater: a current status and limitations. John Wiley & Sons, Chiehester, pp 5–23

Frimmel FH, Abbt-Braun G, Heumann KG, Hock B, Lüdemann H-D, Spiteller M (2008) Refractory organic substances in the environment. Wiley-VCH, Weinheim

Garg S, Rose AL, Waite TD (2011) Photochemical production of superoxide and hydrogen peroxide from natural organic matter. Geochim Cosmochim Acta 75:4310–4320. https://doi.org/10.1016/j.gca.2011.05.014

Gilja V, Novaković K, Travas-Sejdic J, Hrnjak-Murgić Z, Kraljić Roković M, Žic M (2017) Stability and synergistic effect of polyaniline/TiO_2 photocatalysts in degradation of azo dye in wastewater. Nanomaterials 7:412. https://doi.org/10.3390/nano7120412

Gu L, Wang J, Qi R, Wang X, Xu P, Han X (2012) A novel incorporating style of polyaniline/TiO_2 composites as effective visible photocatalysts. J Mol Catal A: Chem 357:19–25. https://doi.org/10.1016/j.molcata.2012.01.012

Heshmatpour F, Zarrin S (2017) A probe into the effect of fixing the titanium dioxide by a conductive polymer and ceramic on the photocatalytic activity for degradation of organic pollutants. J Photochem Photobiol A 346:431–443. https://doi.org/10.1016/j.jphotochem.2017.06.017

Jangid NK, Jadoun S, Yadav A, Srivastava M, Kaur N (2021) Polyaniline-TiO_2-based photocatalysts for dyes degradation. Polym Bull 78:4743–4777. https://doi.org/10.1007/s00289-020-03318-w

Jumat NA, Wai PS, Ching JJ, Basirun WJ (2017) Synthesis of polyaniline-TiO_2 nanocomposites and their application in photocatalytic degradation. Polym Polym Compos 25:507–514. https://doi.org/10.1177/096739111702500701

Korshin GV, Kumke MU, Li C-W, Frimmel FH (1999) Influence of chlorination on chromophores and fluorophores in humic substances. Environ Sci Technol 33:1207–1212. https://doi.org/10.1021/es980787h

Koysuren O, Koysuren HN (2019) Photocatalytic activity of polyaniline/Fe-doped TiO_2 composites by in situ polymerization method. J Macromol Sci A 1–10. https://doi.org/10.1080/10601325.2019.1565548

Laabd M, El Jaouhari A, Chafai H, Bazzaoui M, Kabli H, Albourine A (2016) Experimental and theoretical studies on the removal of polycarboxy-benzoic acids by adsorption onto polyaniline from aqueous solution. Desalination Water Treat 57:15176–15189. https://doi.org/10.1080/19443994.2015.1070288

Lazarevic M, Despotovic V, Sojic-Merkulov D, Banic N, Fincur N, Cetojevic-Simin D, Comor M, Abramovic B (2019) Photodegradation of selected pesticides: photocatalytic activity of bare and PANI-modified TiO_2 under simulated solar irradiation. J Serb Chem Soc 84:1455–1468. https://doi.org/10.2298/JSC190301083L

Lee Y, von Gunten U (2010) Oxidative transformation of micropollutants during municipal wastewater treatment: Comparison of kinetic aspects of selective (chlorine, chlorine dioxide, ferrateVI, and ozone) and non-selective oxidants (hydroxyl radical). Water Res 44:555–566. https://doi.org/10.1016/j.watres.2009.11.045

Lee Y-J, Lee HS, Lee C-G, Park S-J, Lee J, Jung S, Shin G-A (2020) Application of PANI/TiO_2 composite for photocatalytic degradation of contaminants from aqueous solution. Appl Sci 10:6710. https://doi.org/10.3390/app10196710

Li X, Wang D, Cheng G, Luo Q, An J, Wang Y (2008) Preparation of polyaniline-modified TiO_2 nanoparticles and their photocatalytic activity under visible light illumination. Appl Catal B 81:267–273. https://doi.org/10.1016/j.apcatb.2007.12.022

Li Q, Sun L, Zhang Y, Qian Y, Zhai J (2011) Characteristics of equilibrium, kinetics studies for adsorption of Hg(II) and Cr(VI) by polyaniline/humic acid composite. Desalination 266:188–194. https://doi.org/10.1016/j.desal.2010.08.025

Loiselle S, Vione D, Minero C, Maurino V, Tognazzi A, Dattilo AM, Rossi C, Bracchini L (2012) Chemical and optical phototransformation of dissolved organic matter. Water Res 46:3197–3207. https://doi.org/10.1016/j.watres.2012.02.047

Ma J, Dai J, Duan Y, Zhang J, Qiang L, Xue J (2020) Fabrication of PANI-TiO_2/rGO hybrid composites for enhanced photocatalysis of pollutant removal and hydrogen production. Renew Energy 156:1008–1018. https://doi.org/10.1016/j.renene.2020.04.104

Nowakowska M, Szczubiałka K (2017) Photoactive polymeric and hybrid systems for photocatalytic degradation of water pollutants. Polym Degrad Stab 145:120–141. https://doi.org/10.1016/j.polymdegradstab.2017.05.021

Parrino F, Palmisano L (2021) Titanium dioxide (TiO_2) and its applications (Metal Oxides), Elsevier, Netherlands.

Rahman KH, Kar AK (2020a) Effect of band gap variation and sensitization process of polyaniline (PANI)-TiO_2 p-n heterojunction photocatalysts on the enhancement of photocatalytic degradation of toxic methylene blue with UV irradiation. J Environ Chem Eng 8:104181. https://doi.org/10.1016/j.jece.2020.104181

Rahman KH, Kar AK (2020b) Titanium-di-oxide (TiO_2) concentration-dependent optical and morphological properties of PAni-TiO_2 nanocomposite. Mater Sci Semicond Process 105:104745. https://doi.org/10.1016/j.mssp.2019.104745

Reddy KR, Karthik KV, Prasad SBB, Soni SK, Jeong HM, Raghu AV (2016) Enhanced photocatalytic activity of nanostructured titanium dioxide/polyaniline hybrid photocatalysts. Polyhedron 120:169–174. https://doi.org/10.1016/j.poly.2016.08.029

Riaz U, Ashraf SM, Kashyap J (2015) Enhancement of photocatalytic properties of transitional metal oxides using conducting polymers: a mini review. Mater Res Bull 71:75–90. https://doi.org/10.1016/j.materresbull.2015.06.035

Salem MA, Al-Ghonemiy AF, Zaki AB (2009) Photocatalytic degradation of allura red and quinoline yellow with polyaniline/TiO_2 nanocomposite. Appl Catal B 91:59–66. https://doi.org/10.1016/j.apcatb.2009.05.027

Sambaza SS, Maity A, Pillay K (2020) Polyaniline-coated TiO_2 nanorods for photocatalytic degradation of bisphenol A in Water. ACS Omega 5:29642–29656. https://doi.org/10.1021/acsomega.0c00628

Sandikly N, Kassir M, El Jamal M, Takache H, Arnoux P, Mokh S, Al-Iskandarani M, Roques-Carmes T (2021) Comparison of the toxicity of waters containing initially sulfaquinoxaline after photocatalytic treatment by TiO_2 and polyaniline/TiO_2. Environ Technol 42:419–428. https://doi.org/10.1080/09593330.2019.1630485

Sarmah S, Kumar A (2011) Photocatalytic activity of polyaniline-TiO_2 nanocomposites. Indian J Phys 85:713. https://doi.org/10.1007/s12648-011-0071-1

Sboui M, Nsib MF, Rayes A, Swaminathan M, Houas A (2017) TiO_2–PANI/Cork composite: A new floating photocatalyst for the treatment of organic pollutants under sunlight irradiation. J Environ Sci 60:3–13. https://doi.org/10.1016/j.jes.2016.11.024

Senesi N (1990) Molecular and quantitative aspects of the chemistry of fulvic acid and its interactions with metal ions and organic chemicals: Part II. The fluorescence spectroscopy approach. Anal Chim Acta 232:77–106. https://doi.org/10.1016/S0003-2670(00)81226-X

Senesi N, Tm M, Mr P, Brunetti G (1991) Characterization, differentiation, and classification of humic substances by fluorescence spectroscopy. Soil Sci 152:259–271

Sojic Merkulov DV, Despotovic VN, Banic ND, Armakovic SJ, Fincur NL, Lazarevic MJ, Cetojevic-Simin DD, Orcic DZ, Radoicic MB, Saponjic ZV, Comor MI, Abramovic BF (2018) Photocatalytic decomposition of selected biologically active compounds in environmental waters using $TiO_{(2)}$/polyaniline nanocomposites: kinetics, toxicity and intermediates assessment. Environ Pollut 239:457–465. https://doi.org/10.1016/j.envpol.2018.04.039

Sun C, Xiong B, Pan Y, Cui H (2017) Adsorption removal of tannic acid from aqueous solution by polyaniline: analysis of operating parameters and mechanism. J Colloid Interface Sci 487:175–181. https://doi.org/10.1016/j.jcis.2016.10.035

Tercero Espinoza LA, ter Haseborg E, Weber M, Frimmel FH (2009) Investigation of the photocatalytic degradation of brown water natural organic matter by size exclusion chromatography. Appl Catal B 87:56–62. https://doi.org/10.1016/j.apcatb.2008.08.013

Turkten N, Bekbolet M (2020) Photocatalytic performance of titanium dioxide and zinc oxide binary system on degradation of humic matter. J Photochem Photobiol A 401:112748. https://doi.org/10.1016/j.jphotochem.2020.112748

Turkten N, Cinar Z, Tomruk A, Bekbolet M (2019) Copper-doped TiO_2 photocatalysts: application to drinking water by humic matter degradation. Environ Sci Pollut Res Int 26:36096–36106. https://doi.org/10.1007/s11356-019-04474-x

Turkten N, Karatas Y, Bekbolet M (2021) Preparation of PANI modified ZnO composites via different methods: Structural, morphological and photocatalytic properties. Water 13:1025. https://doi.org/10.3390/w13081025

Turkten N, Karatas Y, Uyguner-Demirel CS, Bekbolet M (2023) Photocatalytic performance of PANI modified TiO_2: Preparation and characterization of PANI modified TiO_2 under pre- and post- photocatalytic conditions, to be submitted.

Uyguner CS, Bekbolet M (2005a) Evaluation of humic acid photocatalytic degradation by UV–vis and fluorescence spectroscopy. Catal Today 101:267–274. https://doi.org/10.1016/j.cattod.2005.03.011

Uyguner CS, Bekbolet M (2005b) Implementation of spectroscopic parameters for practical monitoring of natural organic matter. Desalination 176:47–55. https://doi.org/10.1016/j.desal.2004.10.027

Uyguner-Demirel CS, Bekbolet M (2011) Significance of analytical parameters for the understanding of natural organic matter in relation to photocatalytic oxidation. Chemosphere 84:1009–1031. https://doi.org/10.1016/j.chemosphere.2011.05.003

Uyguner-Demirel CS, Birben NC, Bekbolet M (2017) Elucidation of background organic matter matrix effect on photocatalytic treatment of contaminants using TiO_2: a review. Catal Today 284:202–214. https://doi.org/10.1016/j.cattod.2016.12.030

Uyguner-Demirel CS, Turkten N, Kaya D, Bekbolet M (2022) Effect of oxidative and non-oxidative conditions on molecular size fractionation of humic acids: TiO_2 and Cu-doped TiO_2 photocatalysis. Environ Sci Pollut Res 29:85413–85432. https://doi.org/10.1007/s11356-022-21754-1

Wang J, Deng B, Chen H, Wang X, Zheng J (2009) Removal of aqueous Hg(II) by polyaniline: sorption characteristics and mechanisms. Environ Sci Technol 43:5223–5228. https://doi.org/10.1021/es803710k

Wang J, Ding S, Zheng C, Ma H, Ji Y (2012) Efficient removal of humic acid in aqueous solution using polyaniline adsorbent. Desalination Water Treat 40:92–99. https://doi.org/10.1080/19443994.2012.671153

Wang J, Bi L, Ji Y, Ma H, Yin X (2014) Removal of humic acid from aqueous solution by magnetically separable polyaniline: adsorption behavior and mechanism. J Colloid Interface Sci 430:140–146. https://doi.org/10.1016/j.jcis.2014.05.046

Wang N, Li J, Lv W, Feng J, Yan W (2015) Synthesis of polyaniline/TiO_2 composite with excellent adsorption performance on acid red G. RSC Adv 5:21132–21141. https://doi.org/10.1039/C4RA16910G

Wang N, Chen J, Wang J, Feng J, Yan W (2019) Removal of methylene blue by Polyaniline/TiO_2 hydrate: adsorption kinetic, isotherm and mechanism studies. Powder Technol 347:93–102. https://doi.org/10.1016/j.powtec.2019.02.049

Yang C, Dong W, Cui G, Zhao Y, Shi X, Xia X, Tang B, Wang W (2017) Enhanced photocatalytic activity of PANI/TiO_2 due to their photosensitization-synergetic effect. Electrochim Acta 247:486–495. https://doi.org/10.1016/j.electacta.2017.07.037

Zhang H, Zong R, Zhao J, Zhu Y (2008) Dramatic visible photocatalytic degradation performances due to synergetic effect of TiO_2 with PANI. Environ Sci Technol 42:3803–3807. https://doi.org/10.1021/es703037x

Zhang Y, Li Q, Sun L, Tang R, Zhai J (2010) High efficient removal of mercury from aqueous solution by polyaniline/humic acid nanocomposite. J Hazard Mater 175:404–409. https://doi.org/10.1016/j.jhazmat.2009.10.019